PCCP

Effects of Water on the Stochastic Motions of Propane Confined in MCM-41-S Pores

Journal:	*Physical Chemistry Chemical Physics*
Manuscript ID	CP-ART-08-2019-004741.R1
Article Type:	Paper
Date Submitted by the Author:	17-Oct-2019
Complete List of Authors:	Gautam, Siddharth ; Ohio State University, School of Earth Sciences Le, Tran; University College London, Chemical Engineering Rother, Gernot; Oak Ridge National Laboratory, Chemical Sciences Division Jalarvo, Niina; Oak Ridge Na, Chemical and Engineering Materials Divisio Liu, Tingting; The Ohio State University, School of Earth Sciences Mamontov, Eugene; Oak Ridge National Laboratory, Spallation Neutron Source Dai, Sheng; Oak Ridge National Laboratory, Qiao, Zhen-An; Oak Ridge National Laboratory Striolo, Alberto; University College London, Department of Chemical Engineering Cole, David; The Ohio State University, School of Earth Sciences

SCHOLARONE™
Manuscripts

Effects of Water on the Stochastic Motions of Propane Confined in MCM-41-S Pores

Siddharth Gautam[1*], Tran Thi Bao Le[2], Gernot Rother[3], Niina Jalarvo[4], Tingting Liu[1], Eugene Mamontov[4], Sheng Dai[3], Zhen-An Qiao[3], Alberto Striolo[2] and David Cole[1]

[1]School of Earth Sciences, The Ohio State University, 125 S Oval Mall, Columbus, 43210, OH, United States of America

[2]Department of Chemical Engineering, University College London, London WC1E 6BT, United Kingdom

[3]Chemical Sciences Division, Oak Ridge National Laboratory, Oak Ridge, Tennessee 37831, United States of America

[4]Neutron Science Directorate, Oak Ridge National Laboratory, Oak Ridge, Tennessee 37831, United States of America

[*]Corresponding author email: gautam.25@osu.edu

Address: School of Earth Sciences, The Ohio State University, 275 Mendenhall Laboratory, 125 S Oval Mall, Columbus, Ohio, 43210, United States of America

Effect of Water on the Stochastic Motion of Propane Confined in MCM-41-S Pores

Abstract

Hydrocarbons confined in porous media find applications in a wide variety of industries and therefore their diffusive behavior is widely studied. Most of the porous media found in natural environments is laden with water, which might affect the confined hydrocarbons. To quantify the effect of hydration, we report here a combined quasielastic neutron scattering (QENS) and molecular dynamics (MD) simulation study on the dynamics of propane confined in the 1.5 nm-wide micropores of MCM-41-S in presence of water at 230 and 250 K. To eliminate strong incoherent signal from water and emphasize propane signal we have used heavy water (D_2O). QENS data show two dynamically different populations of propane in MCM-41-S and suggest that the presence of water hinders the diffusion of propane. Weak elastic contributions to the QENS spectra suggest that only long-range translational motion of propane molecules contributes to the quasielastic broadening. MD simulations carried out using a model cylindrical silica pore of 1.6 nm diameter filled with water and propane agree with the experimental finding of water hindering the diffusion of propane. Further, the simulation results suggest that the slowing down of propane motions is a function of water content within the pore and is stronger at higher water contents. At high water content, the structure as well as the dynamics, both translational and rotational, of propane are severely impacted. Simulation data suggest that the rotational motion of propane molecule occurs at time scales much faster than those accessible with the QENS instrument used, and thus explains the weak elastic contribution to the QENS spectra measured in the experiments. This study shows the effects of hydration on the structure and dynamics of volatiles in porous media which are of interest for fundamental understanding and applied studies of confined fluids.

1. Introduction

Several industrial sectors, including catalysis and subsurface gas recovery, rely on the diffusive behavior of gases confined in nanoporous materials[1-3]. Of particular interest are hydrocarbons, which show very peculiar behaviors in confinement[4-6]. A significant amount of research effort has been devoted to the study of diffusive behavior of hydrocarbons under confinement in porous materials[7,8]. Both saturated[9-14] and unsaturated[15-19] hydrocarbons with different carbon contents and confined in various media have been studied. Among alkanes, propane offers a unique case. Because of the roughly pentagonal shape of propane molecule, this fluid exhibits the lowest melting point among alkanes[20]. Effects of confinement on several properties of propane have been studied by confining it in porous media differing in both pore shape as well as size[12,13,21-25]. While all these studies have in general found a suppression in the mobility of propane upon confinement, anomalies have been observed in the loading dependence of this suppression[13]. The effect of confinement on the vibrational properties of propane has also been recently documented[26].

Previous work on the effects of confinement on the dynamics of propane focused on idealized systems of single-specie confinement. In natural environments, however, pores are seldom occupied by a single species. While some studies have reported the effects of presence or absence of a second species on the dynamics of one guest[10, 13, 27-30], the most ubiquitous species that can be found in the natural pore environments – water, has largely been ignored. Although the dynamics of confined water has been studied extensively[31,32], the effect of water on the dynamics of another confined species remains largely unexplored. Exceptions include Phan et al.[33] and Bui et al.,[34] who studied the effect of water on the transport of confined methane. Recently, Le et al. reported MD simulation studies on the effect of water on the diffusion of propane in amorphous silica cylindrical pores of diameter 1.6 nm at 300 K[35]. This pore environment resembles the 1.5 nm wide pores in molecular sieve MCM-41-S.

To fill the gaps in our understanding of the behavior of coexisting water and a volatile, we report here a quasielastic neutron scattering (QENS) study on the effect of D_2O on the dynamics of propane confined in MCM-41-S at low temperatures (230 and 250 K). The results of these experiments are complemented by MD simulations which build our previously reported simulation studies[35]. Both experiment and simulations suggest that water hinders the diffusion of propane in MCM-41-S pores. Further, the simulation data show that this hindering effect gets stronger with

91 the water content within the pore. At the highest water content, both the structure and dynamics of

92 the confined propane are severely restricted compared to bulk water.

93 In the remainder of the manuscript, we begin with detailing the experimental and simulation

94 procedures implemented in Section 2. This is followed by defining some important quantities

95 obtained from QENS experiments and MD simulations, and by detailing the connection between

96 experiments and simulations in Section 3. Results from the QENS experiment are described in

97 Section 4.1 while the structural and dynamical properties of the confined propane obtained from

98 MD are reported in Section 4.2. In Section 5, the results from the experiments and the simulations

99 are compared and discussed in connection with relevant literature studies. Finally, we present

100 conclusions in Section 6. Our focus is on the properties of confined propane, while water will be

101 treated as a medium whose principle function is to compete with propane.

102

2. Experimental and Simulation Details

103

104 **2.1 Samples:** The MCM-41-S sample used in the experiment was synthesized at Oak Ridge

105 National Laboratory[26]. For this, Tetraethyl orthosilicate (TEOS) was added to a vigorously stirred

106 solution of amine in ethanol and deionized water, yielding a reaction mixture of the following

107 molar composition: 1.0 TEOS:0.27 $C_8H_{17}NH_2$:9.09 EtOH:29.6 H_2O. The reaction mixture was

108 aged at ambient temperature for 18 h to obtain the hexagonal mesoporous silica. All ambient

109 temperature syntheses were conducted by exposing the reaction mixture to the open atmosphere.

110 Small amounts of deionized water were added during the aging process to compensate for the

111 evaporation. The obtained crystalline products were recovered by filtration, washed with deionized

112 water, and air-dried. Template removal was achieved either by calcination in air at 630 °C for 4 h

113 (heating rate 2 °C/min) or by solvent extraction. The MCM-41-S sample thus synthesized had a

114 bimodal pore distribution with pores of diameter 1.5 nm along with some pores of diameter 2.2

115 nm. The sample surface area, determined with N_2 adsorption at 77 K (BET), was 832 m^2/g and its

116 pore volume 1.2 cm^3/g. More details about sample characterization have been reported in an earlier

117 publication[26].

118 **2.2 Experiment:** The Quasielastic Neutron Scattering (QENS) experiment was carried out using

119 the backscattering instrument BASIS at the Spallation Neutron Source (SNS), Oak Ridge National

120   Laboratory (ORNL), Tennessee[36]. This instrument provides an elastic line resolution of 3.5 µeV

121   at full width at half-maximum and an energy transfer window of +/- 120 µeV. 1 gm of MCM-41-

122   S sample (1.5 nm pores) was loaded into a cylindrical aluminum cell 6 mm in diameter and

123   evacuated using a vacuum pump to remove any residual proton species. Propane gas was pumped

124   into the sample using a high-pressure syringe pump at a pressure of 1 bar, measured at 300 K. The

125   pressure in the sample cell was monitored using a pressure gauge on the capillary supplying the

126   gas to it. After loading propane, the sample cell was isolated and cooled to lower temperatures.

127   Note that cooling the sample cell resulted in a lowering of the sample cell pressure. As propane

128   pressure corresponded to vapor densities at all times, the sample thickness was of optimal

129   dimension to avoid multiple scattering. To study the effect of water on the dynamics of confined

130   propane, another MCM-41-S sample, hydrated with D_2O (10% by weight of D_2O in MCM-41-S)

131   was used in separate QENS measurements. We note that this water loading does not quantify the

132   amount of water that penetrated the pores. The difference between the two samples used in the

133   QENS experiments is thus mainly in terms of presence or absence of water in the pores.

134   Measurements were taken at the temperatures 250 K, 230 K and 10 K. The lowest temperature

135   measurement was used to define the instrumental resolution. Spectra of hydrated as well as

136   dehydrated MCM-41-S were subtracted from the respective propane loaded spectra to account for

137   silica and water background. This subtraction also removes any contribution to the QENS spectra

138   from the silanol groups on the pore surface. The subtracted spectra thus represent signals from

139   propane alone. QENS data were reduced and analyzed using the software package DAVE[37].

140   **2.3 Simulations:** The preparation of the simulation cell used in this work has been described

141   elsewhere[35]. It consisted of two stages – preparing a cylindrical pore of amorphous silica, and then

142   loading water and propane molecules in this pore. For the first stage, a β-cristobalite supercell was

143   melted at 7000 K, equilibrated in the liquid state and then quenched by cooling it at a rate of 4

144   K/ps to 300 K. A cylindrical pore of diameter 16 Å was then carved out from the simulation cell

145   by removing all atoms that lay within 8 Å from the X-axis. The resulting pore was oriented along

146   X-axis. Removing atoms in this manner resulted in dangling Si and O atoms. These were saturated

147   with hydroxyl groups and hydrogen atoms, respectively. In the second stage, a desired number of

148   water and propane molecules were placed at each side of the cylindrical pore, along the X direction.

149   As simulations proceeded, water and propane spontaneously filled the pore and distributed across

150   both pore and bulk volumes. Once equilibrium is reached, the propane density in the bulk was

151 calculated from density profiles along the X-direction. The reservoir was removed after fluid

152 molecules corresponding to the appropriate densities were adsorbed in the pore. More details on

153 the two stages of sample preparation can be found elsewhere[35].

154 To prepare the model MCM-41-S using the melting of a β-cristobalite crystal as outlined above,

155 we used the Morse-type potential developed by Demirlap et. al.[38] to model the interaction between

156 Si and O atoms. Once the MCM-41-S model pore was prepared, the substrate was modeled using

157 the CLAYFF[39] force field in all subsequent simulations. Water molecules were modeled with

158 TIP4P/Ice[40] force field while TraPPE-UA[41] force field was used to model propane molecules.

159 Following the TraPPE-UA convention, all interactions were cut-off at 14 Å. Long range

160 electrostatic interactions were treated with the particle mesh Ewald (PME)[42] method and Lorentz-

161 Berthelot mixing rules were used to estimate the parameters for cross-terms[43]. Periodic boundary

162 conditions were applied in all directions. This resulted in an infinitely long cylindrical pore along

163 the Cartesian X direction.

164 Several different fluid compositions were simulated to systematically study the effect of water on

165 the dynamics of confined propane. The initial number of propane molecules adsorbed in the pore

166 was determined by GCMC simulations at 1 bar and 300 K to match the experimental conditions at

167 the time of gas loading in the experiments. However, the amount of propane (5 molecules) was

168 too small for extracting quantities with good statistics, therefore a slightly higher propane loading

169 of 22 molecules was used in the simulation cell. Several water loadings were used, as summarized

170 in Table 1. Each of the samples listed in Table 1 were simulated at 230 and 250 K. As noted earlier,

171 the focus of this paper is on the dynamics of propane. Quantities used for comparison between the

172 experiments and simulations (i. e., intermediate scattering functions) were calculated for the

173 systems Dry and Hydrated 1 (D and H1 in Table 1) at 230 K. All simulated systems were

174 equilibrated for 80-100 ns before a production run of 2 ns. The production run was limited to 2 ns

175 as our intention was to mainly compare the simulations with QENS experiments which probe time

176 scales below 1 ns. The production run was repeated up to 3 times, and no significant deviation was

177 observed in the results obtained.

178

179

180   **Table 1**. System composition (number of propane and water molecules) for our MD simulations

181   in model MCM-41-S pore.

Simulation Sample	Number of Propane molecules	Number of water molecules
Dry (D)	22	0
Hydrated 1 (H1)	22	221
Hydrated 2 (H2)	22	271
Hydrated 3 (H3)	22	321
Hydrated 4 (H4)	22	362

182

183

184   ## 3. Important quantities and connection between QENS and MD

185   simulations

186   QENS and MD simulations are often used in combination to study the stochastic motion of

187   molecules[7]. This is because both techniques access similar length and time scales[7], although

188   advances in computations have made the range of length and time scales accessible to MD

189   simulations relatively larger and longer respectively. The self-diffusion coefficient (D) is obtained

190   from QENS experiments by analyzing the broadening of an elastic line due to the stochastic

191   motions constituting self-diffusion[44]. From MD simulations, D can be obtained from the long-time

192   slope of mean squared displacement (MSD) vs time plots[43]:

193    $$D = \lim_{t \to \infty} \frac{\langle |r_i(t+t_0) - r_i(t_0)|^2 \rangle}{2n_d t} \qquad (1)$$

194   In Eq. (1), the quantity in the numerator is the MSD, with $r_i(t + t_0)$ and $r_i(t_0)$ being the positions of

195   the ith entity (atoms or molecules) at times $t + t_0$ and t_0, respectively; the angular brackets denote

196   ensemble average. The quantity n_d in the denominator stands for the number of degrees of freedom.

197   Typically, center of mass positions of the molecules are used for r_i.

198   In our previous study[23], we showed that a more direct comparison can be made between the QENS

199   experiments and MD simulations by calculating quantities that are directly related to the observed

200   signal in the QENS experiments from the simulated trajectories. In a QENS experiment on a

201   sample with hydrogen atoms, the observed signal is proportional to the incoherent scattering law

202     $S_{inc}(Q,\omega)$, a quantity that encodes information on the structure and dynamics in the sample by

203   virtue of its dependence on Q and ω, respectively[*]. The incoherent scattering law is a Fourier

204   transform of the self-intermediate scattering function (ISF), $I(Q,t)$. ISF can be directly calculated

205   from the simulated molecular trajectories using the expression

206     $$I(Q,t) = \langle \exp\left(i\boldsymbol{Q}.[\boldsymbol{r_i}(t+t_0) - \boldsymbol{r_i}(t_0)]\right) \rangle \tag{2}$$

207   In Eq. (2), $i=\sqrt{-1}$ and averages are carried out over all atoms/molecules and time origins t_0 and

208   different $\boldsymbol{Q}$ with the same magnitude. The last averaging is the powder averaging necessary for

209   comparisons to experiments using powder samples with no preferred orientation. Further, this

210   function can be calculated for contributions from translational and rotational motions by separating

211   the co-ordinates of an interaction site (for example CH_3) ($\boldsymbol{r}$) into co-ordinates of the center of mass

212   (COM) of the molecules ($\boldsymbol{r_{COM}}$) and co-ordinates of that site in the center of mass frame ($\boldsymbol{d}$). Thus,

213     $$\boldsymbol{r} = \boldsymbol{r_{COM}} + \boldsymbol{d} \tag{3}$$

214   Purely translational motion of the molecules can be studied by following the evolution of $\boldsymbol{r_{COM}}$ in

215   time, whereas rotational motion can be studied by following the evolution of a unit vector ($\boldsymbol{e}$) along

216     $\boldsymbol{d}$ in time. Self-intermediate scattering functions for the two motions can be calculated by replacing

217     $\boldsymbol{r}$ in Eq. 2 by $\boldsymbol{r_{COM}}$ to obtain the translational intermediate scattering function (TISF) and by $\boldsymbol{e}$ to

218   obtain rotational intermediate scattering function (RISF).

219   The scattering law obtained from QENS experiments on a diffusive system is often modeled with

220   a Lorentzian function to represent the quasielastic broadening[44]. The corresponding model in the

221   inverse Fourier space for the ISF is therefore an exponential decay function, as a Lorentzian and

222   exponential decay function form a Fourier transform pair. Thus,

223     $$S_{inc}(Q,\omega) \sim L(\Gamma(Q),\omega) \sim \frac{\Gamma(Q)}{(\Gamma^2(Q)+\omega^2)} \quad \Longleftrightarrow \quad I(Q,t) \sim e^{-t/\tau(Q)} \tag{4}$$

---

[*] $\boldsymbol{Q}=\boldsymbol{k_i}-\boldsymbol{k_f}$ is the wave-vector transfer in the event of scattering of the neutron by a sample under study, $\boldsymbol{k_i}$ and $\boldsymbol{k_f}$ being the wave-vector of the neutron before and after the scattering and $\hbar\omega$ is the energy transfer that occurs between the neutron and the sample on a scattering event. $\hbar$ is the reduced Planck constant.

224   In Eq. (4), $L(\Gamma(Q), \omega)$ is a Lorentzian function of ω, centered at $\omega=0$ and its half-width at half-

225   maximum (HWHM) is $\Gamma(Q)$. The exponential decay function $e^{-t/\tau(Q)}$ is characterized by the decay

226   time constant $\tau(Q)$ which is related to the HWHM of the corresponding Lorentzian function as

227    $$\Gamma(Q) = \frac{\hbar}{\tau(Q)} \tag{5}$$

228   Thus, for a diffusive system, the decay constant obtained from modeling the simulated ISF with

229   an exponential decay can be converted to a corresponding energy using Eq. (5), which is directly

230   comparable with the HWHM of the Lorentzian used to model the experimentally measured

231   scattering law.

232   Another important quantity that can be calculated from the simulated trajectories is the rotational

233   correlation function (RCF). RCF can be used to assess the rotational motion of molecules and

234   obtain the relevant time scales. RCF can be calculated using the following expression

235    $$RCF = \langle \boldsymbol{e}_i(t + t_0) \cdot \boldsymbol{e}_i(t_0) \rangle \tag{6}$$

236   In Eq. (6), angular brackets denote ensemble averages, and $\boldsymbol{e}_i$ is a unit vector rotating with molecule

237   i. In the present case we use a unit vector along the CH_3-CH_2 vector of a propane molecule.

238

239   ## 4. Results

240   **4.1 QENS experiments**

241   Figure 1 shows a comparison of the spectra obtained from propane in (a) dry and (b) hydrated

242   (with D_2O) MCM-41-S sample at 230 and 250 K. Also shown are the spectra of a Vanadium can

243   measured at 300 K, which serves as a measure of the instrumental resolution, and evacuated MCM-

244   41-S, also measured at 300 K. The spectrum of evacuated MCM-41-S is almost congruent with

245   that of Vanadium, suggesting an absence of a mobile hydrogen bearing species in MCM-41-S.

246   When D_2O is added to this evacuated sample and the sample cell is cooled to 10 K, the resulting

247   spectrum (shown in (b)) is congruent with the Vanadium spectrum too, and hence can be used to

248   account for the instrument resolution. A comparison of the spectra of propane in dry and moist

249   samples demonstrates that addition of D_2O decreases the quasielastic broadening in the signal

250   produced by the stochastic motion of propane molecules. Hence, our experiments confirm that

251   addition of D_2O suppresses the motion of propane in MCM-41-S.
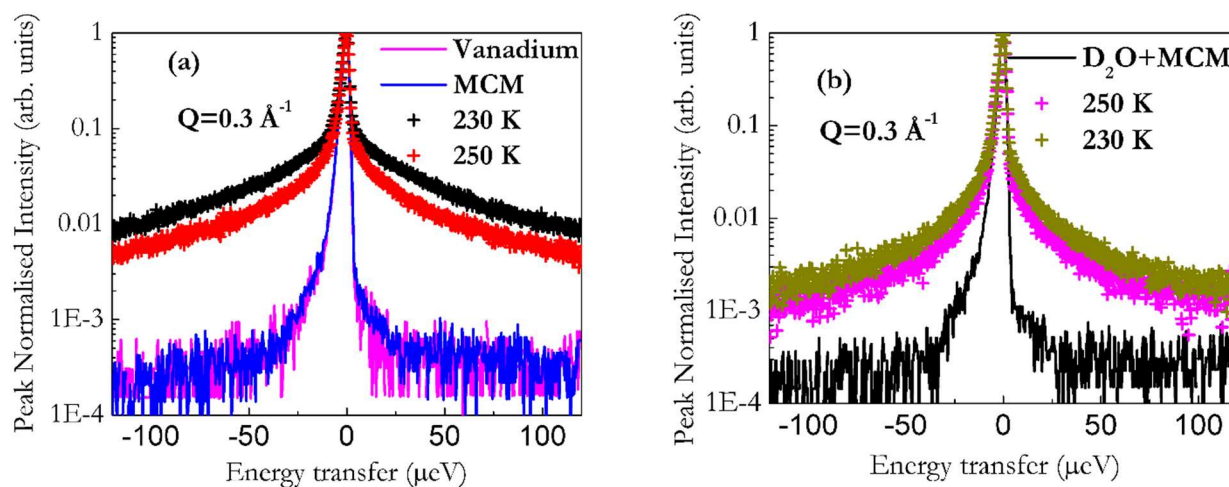
252

253   **Figure 1**. Peak normalised spectra obtained from the QENS experiments on propane in (a) dry,

254   and (b) hydrated (with D_2O) MCM-41-S at Q=0.3 Å^{-1} at two temperatures 230 and 250 K. Also

255   included in the plot are the spectra collected for a Vanadium and bare MCM-41-S measured at

256   300 K (shown in panel (a)) and empty hydrated MCM-41-S measured at 10 K (panel (b)). The

257   effect of D_2O on the mobility of propane in MCM-41-S can be seen as a suppression of

258   quasielastic broadening (data shown with '+' symbols) in the panel (b) as compared to panel (a).

259

260   QENS data analysis was performed to quantify the suppression of propane motion in MCM-41-S

261   upon addition of D_2O. As mentioned earlier, to obtain QENS data that represented only propane,

262   the spectra for dry MCM-41-S were subtracted from the spectra for propane in MCM-41-S and

263   the spectra for D_2O-loaded MCM-41-S were subtracted from the spectra for propane in D_2O-

264   loaded MCM-41-S. It is common practice to describe the $S_{inc}(Q,\omega)$ as composed of an elastic and

265   a quasielastic component along with a background. This $S_{inc}(Q,\omega)$ is convoluted with the

266   instrumental resolution. In case of diffusive motion, the quasielastic part has a Lorentzian profile.

267   The model $S_{inc}(Q,\omega)$ can thus be written as:

268    $S_{inc}(Q,\omega) = \{A(Q)\delta(\omega) + (1 - A(Q))L(\Gamma(Q),\omega) + B(Q,\omega)\} \otimes R(Q,\omega)$ \hfill (7)

Physical Chemistry Chemical Physics

269   In Eq. (7), the first term on the right side is the elastic contribution, which is approximated by a

270   delta function located at zero energy transfer; $A(Q)$ is the fraction of scattering that is elastic, which

271   is called elastic incoherent structure factor (*EISF*). The second term on the right side is the

272   quasielastic component, represented by a Lorentzian function centred at zero energy transfer with

273   a half-width at half-maximum (*HWHM*) of $\Gamma(Q)$. The third term is the background, while $R(Q,\omega)$

274   is the instrument resolution. Fitting the experimental spectra with Eq. (7) did not result in good

275   quality of fits for any propane spectra. Therefore, a combination of two Lorentzians was used to

276   describe the quasi-elastic component for propane. The resulting fitting equation was

277    $S_{inc}(Q,\omega) = \{A(Q)\delta(\omega) + (1 - A(Q))[L_1(\Gamma_1(Q),\omega) + L_2(\Gamma_2(Q),\omega)] + B(Q,\omega)\} \otimes R(Q,\omega)$

278   (8)

279   Good quality fits were obtained using Eq. (8), shown in Figure 2. The need for two Lorentzians to

280   describe the quasielastic part of the spectra of both dry and hydrated samples indicates the presence

281   of two populations of propane molecules, which move at different time scales. The faster one of

282   these populations is represented by the Lorentzian with a broader profile (large $\Gamma(Q)$ values), while

283   the slower population is described by the Lorentzian with narrower profile (smaller $\Gamma(Q)$ values).

284   The fitting parameters $A(Q)$, $\Gamma_1(Q)$ and $\Gamma_2(Q)$ were analysed further, as discussed below.

285   Very low values of $A(Q)$ were obtained from the fits of all the experimental spectra. This indicated

286   an absence of localised motion, or a population of immobile propane molecules in both dry and

287   hydrated MCM-41-S. Fitting of Eq. (8) revealed $\Gamma_1(Q) < \Gamma_2(Q)$, where the former represents slow

288   motion while the latter represents fast motion. The variation of $\Gamma_1(Q)$ and $\Gamma_2(Q)$ obtained from the

289   fits of different propane spectra with Q^2 are shown in Figure 3. These variations are characteristic

290   of a jump diffusion mechanism. In particular, the Singwi-Sjölander model of jump diffusion

291   provides an adequate description of this behavior. In this model, motion occurs via jumps: wherein

292   a molecule sits at a particular site for a time equal to the residence time, τ, before jumping to

293   another site, almost instantaneously. In this model, the $\Gamma(Q)$ varies according to the following

294   relation[45]:

295    $\Gamma(Q) = \dfrac{DQ^2}{1+DQ^2\tau}$ (9)

296   The variations of $\Gamma_1(Q)$ and $\Gamma_2(Q)$ were fitted with Eq. (9) and the obtained parameters – self-

297   diffusion coefficients (D) and residence times (τ) are shown in Fig. 4. Effects of water on the

298   dynamics of confined propane are reduction of the diffusion coefficients (top panels) and

299   corresponding lengthening of residence times (bottom panels) of both components in hydrated

300   samples. The enhancement of motions at higher temperature is seen in all cases except for the slow

301   component of the hydrated sample (indicating a counter-intuitive suppression of mobility at higher

302   temperature). However, we note that the error bars on both the diffusion coefficient and residence

303   time values are rather large making the interpretation of temperature effects on the experimental

304   data less certain. However, the variations of quantities with hydration is larger than the error bars

305   and suggest a clear suppression of propane mobility due to presence of water.
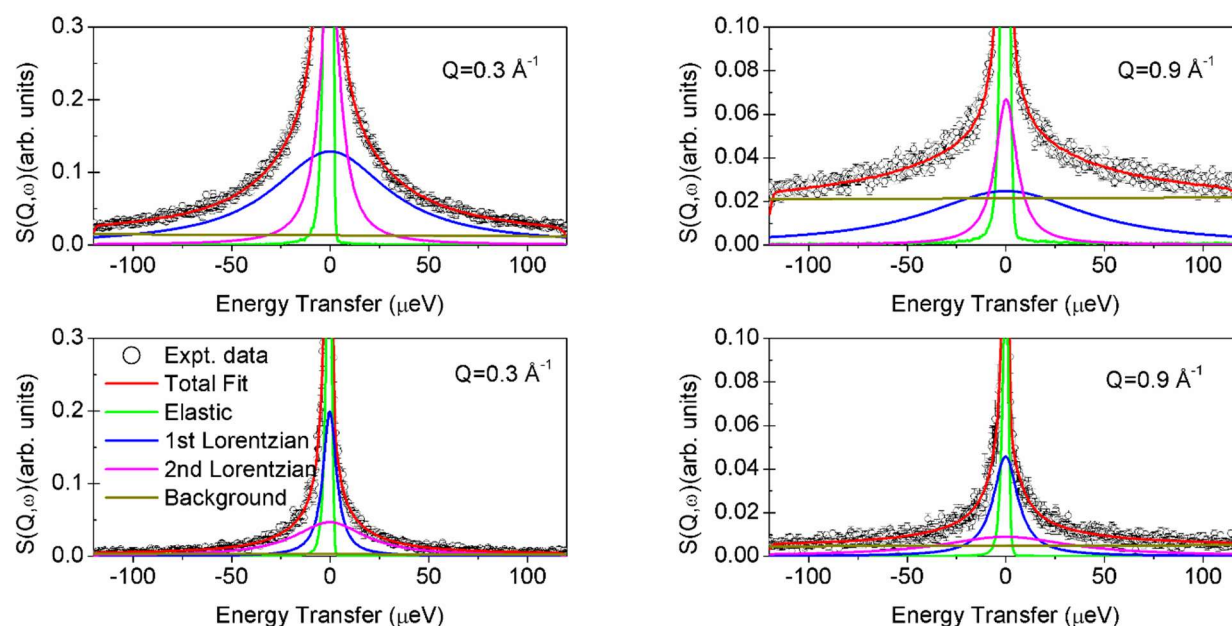
306

307   **Figure 2**. QENS spectra fitted with Eq. (8) for propane in dry (top) and hydrated (bottom)

308   MCM-41-S at 250 K. The left panels show the spectra at $Q =0.3$ Å^{-1}, while the right panels show

309   those at $Q =0.9$ Å^{-1}. The experimental data are shown in symbols, the overall fits in red lines.

310   Different components of the fits are shown in lines with different colors, as shown.

311

Physical Chemistry Chemical Physics

312
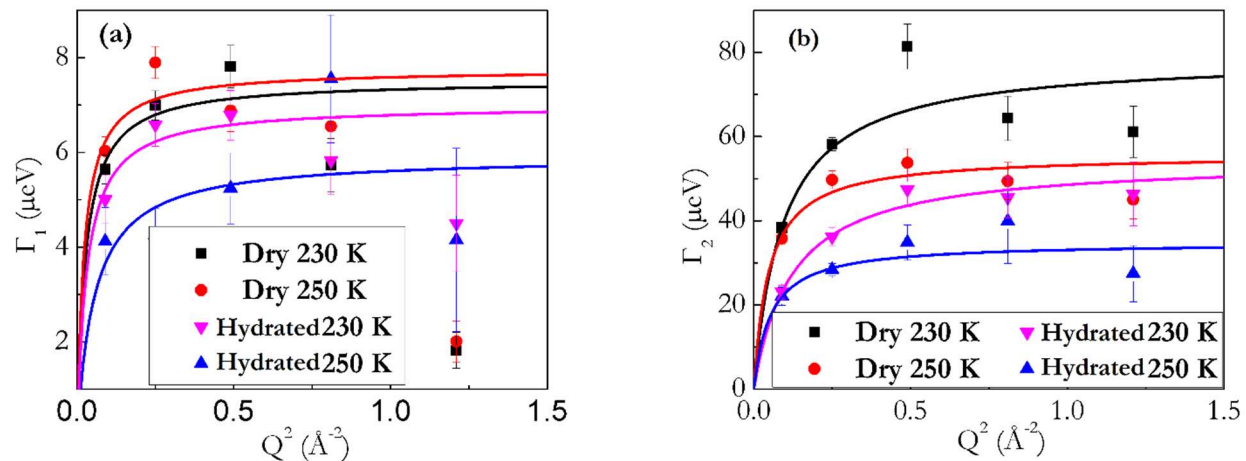
Figure 3. Variation of (a) $\Gamma_1(Q)$ and (b) $\Gamma_2(Q)$ obtained from fitting the QENS spectra of propane in dry and hydrated MCM-41-S at 230 and 250 K, to Eq. (9). The solid lines show the fits of the $\Gamma(Q)$ variation to the jump diffusion model.

316
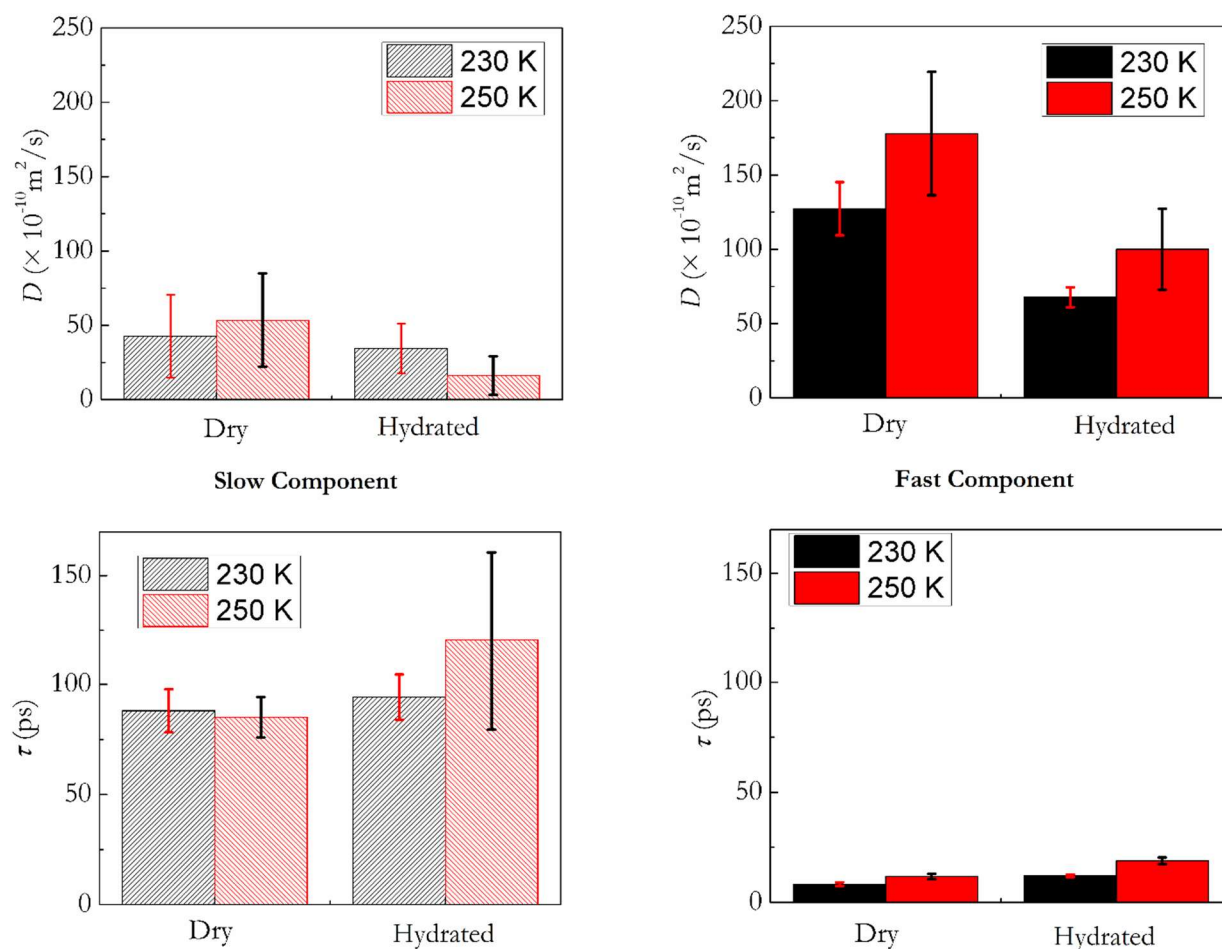
317

318   **Figure 4**. Values of D (top) and τ (bottom) obtained from fitting of the variation of $\Gamma_1(Q)$ and

319      $\Gamma_2(Q)$ with Eq. (9) for propane in dry and hydrated MCM-41-S at 230 and 250 K. The values in

320   the right panel are obtained from the fast component of motion, while those in the left panel are

321   from the slow component.

322

4.2 MD Simulations

324   Figure 5 shows the distribution of molecular propane density in the model MCM-41-S pore in the

325   radial and axial directions at 230 K. The corresponding atomic density distributions for oxygen

326   atoms of water are shown in Figure S1 in the Supplementary Information. To calculate these

327   density profiles, center of mass positions of all propane molecules are recorded at all times and

328   averaged over 4-7 independent simulations. In the case of dry pore, propane molecules arrange

329   themselves in a layer close to the pore surface, peaking at around 4.8 Å from the pore axis. As a

330   low amount of water is introduced in the pore (H1), the peak in propane density is shifted towards

331   the pore axis, as water molecules preferentially adsorb at the pore surface because of their polar

332   nature. Even though the position of the molecular layer of propane is shifted by water, no other

333   pronounced density peak can be seen. As more water is added to the pore (H2), a new second

334   propane layer begins to form close to the pore axis, at the expense of the layer closer to the pore

335   surface. At higher water loadings (H3 and H4), the layers close to the pore axis get denser, because

336   water pushes away propane from the pore surface. Further, at high water contents the propane

337   density profiles are characterised by sharper peaks. In the axial direction, shown in panel (b), the

338   propane molecules are distributed evenly throughout the length of the dry pore as evidenced by an

339   almost featureless flat distribution shown by the red curve. As water is added, a more uneven

340   distribution can be observed (green curve, H1) with more peaks in the central region. As more

341   water is present, the distribution exhibits sharper and more numerous peaks. At highest water

342   content (H4), the large amount of water forces propane molecules to cluster together, yielding

343   layers along the axial direction. A tendency of 'ordering' in the orientational distribution of

344   propane molecules is also observed at high water content (see Supplementary Information, Figure

345   S2). This can be due to the propane molecules being trapped by water molecules, suggesting that

346   ordering is promoted in this system by low mobility of propane molecules. A similar tendency of

347 nanopore ordering due to low mobility has also been observed for acetone, acetaldehyde and

348 acetonitrile in ZSM-5[25].
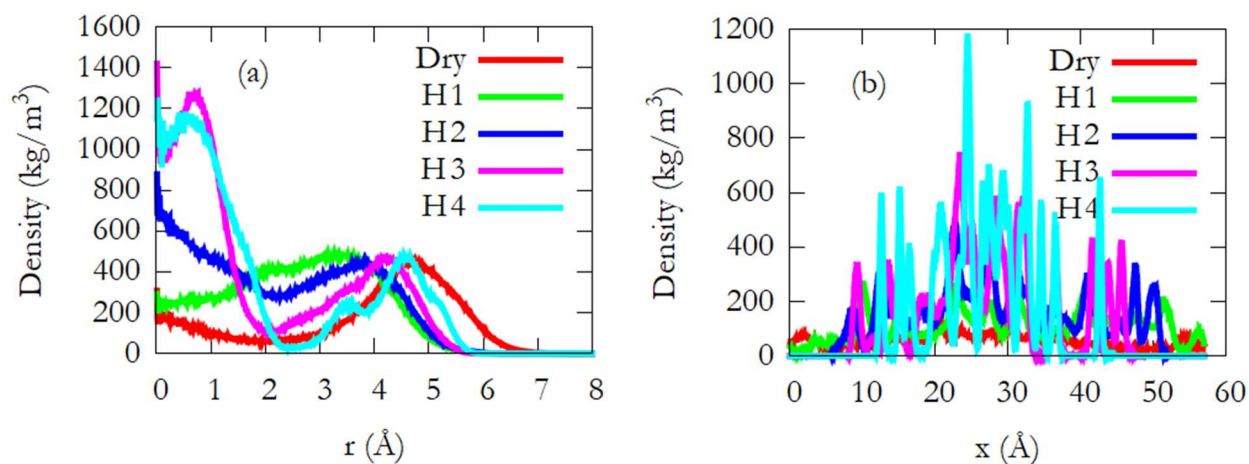
349

350 **Figure 5**. Density distribution of propane molecules in a model MCM-41-S pore along the (a)

351 radial and (b) axial directions. The pore is centered at r=0 Å while in the axial direction the

352 simulation cell boundaries are located at x=0 and 56.9 Å.

353

354 Figure 6 (a) shows the mean squared displacement (MSD) of the center of mass of propane

355 molecules in the model MCM-41-S pore at 230 K. The results are shown as a function of water

356 content. Similar results obtained at 250 K for propane can be found in the Supplementary

357 Information (Figure S3). The MSD of propane at long times gets suppressed with water content in

358 the pore, indicating suppression of mobility. At the highest water content (H4), the MSD plateaus

359 quickly to a constant value, and does not show any appreciable increase after about 0.5 ps. The

360 overall MSD at 230 K in the case of dry sample has also been resolved in three Cartesian directions.

361 As the pore is oriented along the Cartesian X-direction, the overall MSD is almost completely

362 described by the MSD along X-direction (see Supplementary Information, Figure S4). At very

363 short times, the values of MSD along all directions are similar. This is the ballistic regime, where

364 the molecules move freely before colliding against other molecules. At intermediate times, because

365 of layered structure of the fluids, a typical molecule is more likely to collide with another molecule

366 along the radial direction in the pore (Cartesian Y or Z) and so the value of MSD along these

367 directions is suppressed because of more frequent collisions. At longer times, the finite size of the

368 pore along the radial direction puts an absolute limit on the mobility of molecules in this direction,

369   and the molecules are unable to move a squared distance of more than $\sim 20\,\text{Å}^2$. This limit is reached

370   at ~ 50 ps. After this time, motion along the pore axis is solely responsible for the increase of MSD

371   with time and the corresponding motion is represented by 1-D diffusion. The MSD along the pore

372   axis for all systems at 230 K is shown in Figure 6 (b).

373
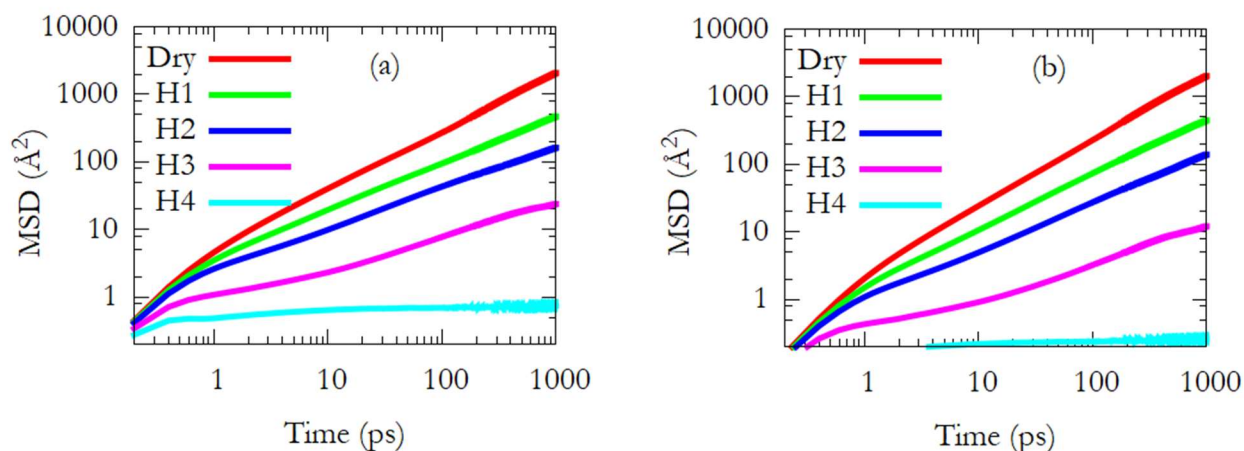
374

375   **Figure 6** (a) Mean squared displacements of the center of mass of propane molecules in model

376   MCM-41-S pore with different moisture contents at 230 K. (b) MSD along the axial direction

377   (Cartesian direction X) at 230 K.

378

379   1-dimensional diffusion coefficients have been obtained from the long-time slope of the MSD

380   along X-direction vs time plots using Eq. 1 and are listed in Table 2. The diffusive nature of motion

381   at long times was ascertained by examining the slope of ln(MSD) vs ln(t) plot. The slopes of these

382   plots for all the systems, except H4, were found to be close to 1 at long enough times, indicating

383   diffusive motion. As the motion of propane molecules in the simulation H4 is severely constrained

384   and not diffusive, no reliable diffusion coefficient is obtained from this simulation. Dynamics of

385   water at the temperatures reported here was severely constrained. However, water molecules in all

386   the systems except H4 exhibited mobility. Water mobilities were reduced by a factor of ~ 10

387   compared to those at 300 K reported earlier[35] (see Supplementary Information, Table S1).

388

Physical Chemistry Chemical Physics

389 **Table 2**. 1-dimensional diffusion coefficients of propane in the systems listed in Table 1. For the

390 system H4 it was not possible to extract reliable values for the propane self-diffusion coefficient

391 because in this system the motion is sub-diffusive even at long times.

Sample	D ($\times 10^{-10}$ m^2/s)	
	230 K	250 K
Dry	99.5±3.1	122.1±3.4
H1	14.8±0.6	20.4±0.7
H2	6.1±0.3	7.6±0.3
H3	0.5±0.1	0.7±0.2
H4	-	-

392

393 As discussed above, to properly connect with the QENS experiments, it is desirable to extract the

394 TISF from the simulated trajectories. Figure 7 shows the TISF at Q = 0.99 Å^{-1} calculated from

395 different simulations at 230 K. Higher water loading results in a slower TISF decay, i.e., slower

396 motions of propane. The time range accessible with the BASIS instrument used in the QENS

397 experiment is highlighted in color in Figure 7. Within this time range, the TISF for most

398 compositions appears to exhibit at least two behaviors. These two behaviors can best be interpreted

399 by consideration of the existence of two dynamical populations of propane molecules, which is

400 consistent with the experimental data. Expanding on this comparison further, the TISF calculated

401 from simulations for dry and H1 compositions can be fitted with exponential decay functions in

402 the time range from 3 to 200 ps, accessible to instrument, in order to estimate the time scales

403 involved in the motion represented by these functions. As noted earlier (Section 3), these time

404 scales can be converted to corresponding $\Gamma^s_i(Q)$ (i=1, 2; superscript 's' is used to indicate quantities

405 obtained from the simulation data) using Eq. (5) and can be compared with $\Gamma_1(Q)$ and $\Gamma_2(Q)$

406 obtained from the QENS experiments. As the quasielastic spectra were fitted with two Lorentzians,

407 the TISF were fitted with two exponential decay functions as well. This translates to fitting

408 ln(TISF) vs. time plot with a combination of two linear functions[†]. The slope of these two lines

409 yields the time scales (τ).

[†] TISF~e$^{(-t/\tau)}$ is equivalent to ln[TISF]~(-t/τ) and hence ln[TISF] vs time is a straight line with slope =(-1/τ)

410
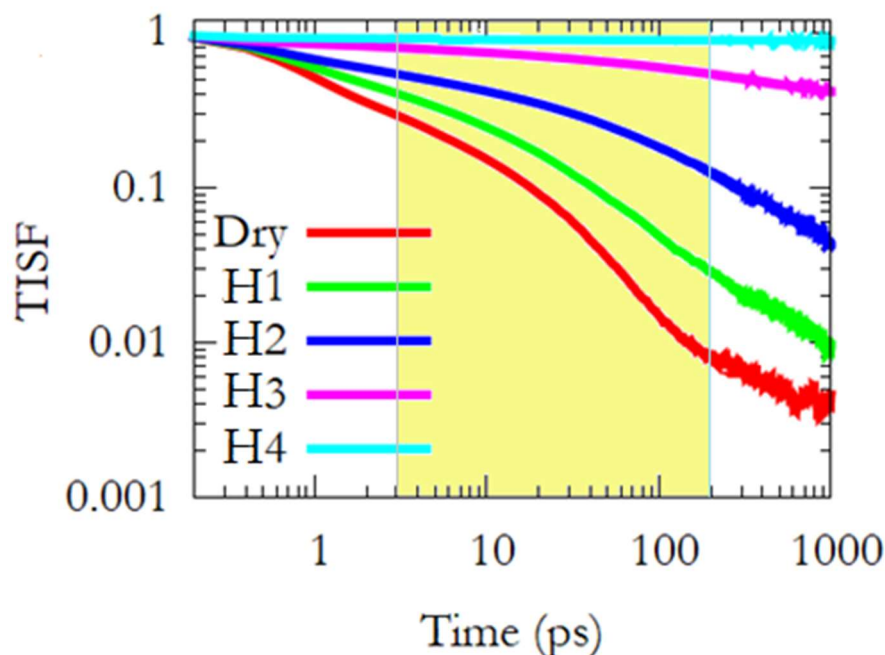
Figure 7. TISF as a function of time calculated from the trajectories of center of mass of propane molecules using Eq. (2) from simulations conducted at 230 K. All TISFs shown are calculated at $Q=0.99$ Å^{-1}. The time range accessible to the instrument used in the experiment is highlighted in colour.

415

Representative ln(TISF) vs. time curves for Dry and H1 systems at 230K are shown in Figure 8. The initial, very fast, decay that lasts for ~ 1 ps represents very fast motion and is out of the time range of the instrument. Beyond that, the ln(TISF) can be divided into two regions with varying slopes. To maintain consistency, all ln(TISF) vs. time plots were fitted within the two ranges of 3-60 ps and 100-200 ps with linear functions. The $\Gamma^s_i(Q)$ ($i=1, 2$) obtained from the fits for the two compositions are shown in Figure 9 as functions of Q^2. As in the experiments, the variation of $\Gamma^s_i(Q)$ with Q^2 is further fitted with a jump diffusion model (Eq. (9)) to obtain diffusion coefficients and residence times. The values of these parameters obtained from the fits are listed in Table 3. The magnitude of the parameters is consistent with those obtained from the experiments. The small quantitative differences result from the difference in compositions used in the experiment and the simulations, along with other typical computational limitations, including the implementation of a generic force field which has not been optimised to reproduce the experiments reported here.
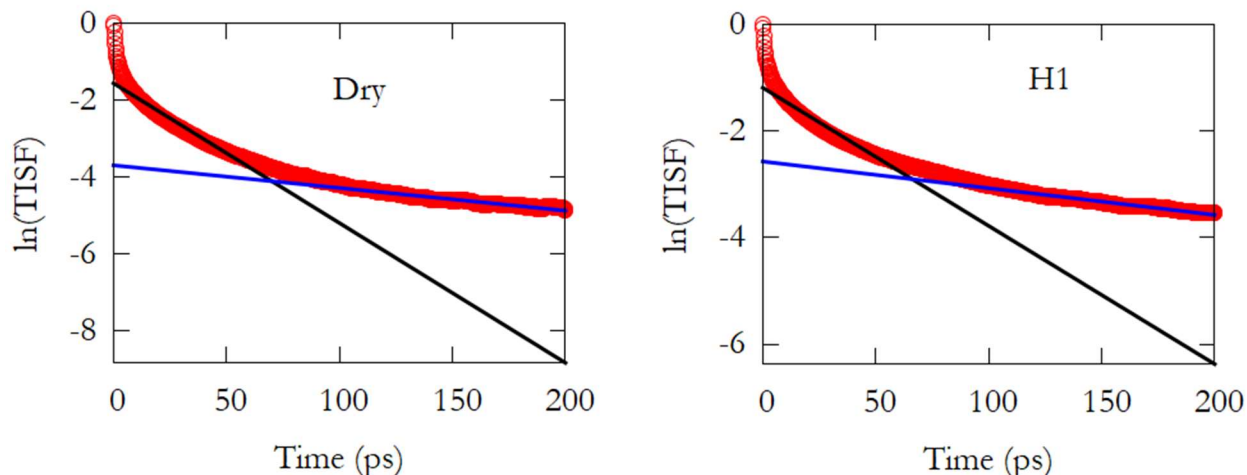
428

429   **Figure 8**. Fits of the simulation derived ln(TISF) vs. t curves in two different time ranges (3-60

430   ps and 100-200 ps) with linear functions. The slope of the fitted linear functions are proportional

431   to $\Gamma^s_i(Q)$ (i=1, 2), which can be directly compared with the HWHM of the Lorentzians

432   representing the quasielastic width ($\Gamma_1(Q)$ and $\Gamma_2(Q)$ shown in Figure 3) as obtained from the

433   QENS experiment.

434
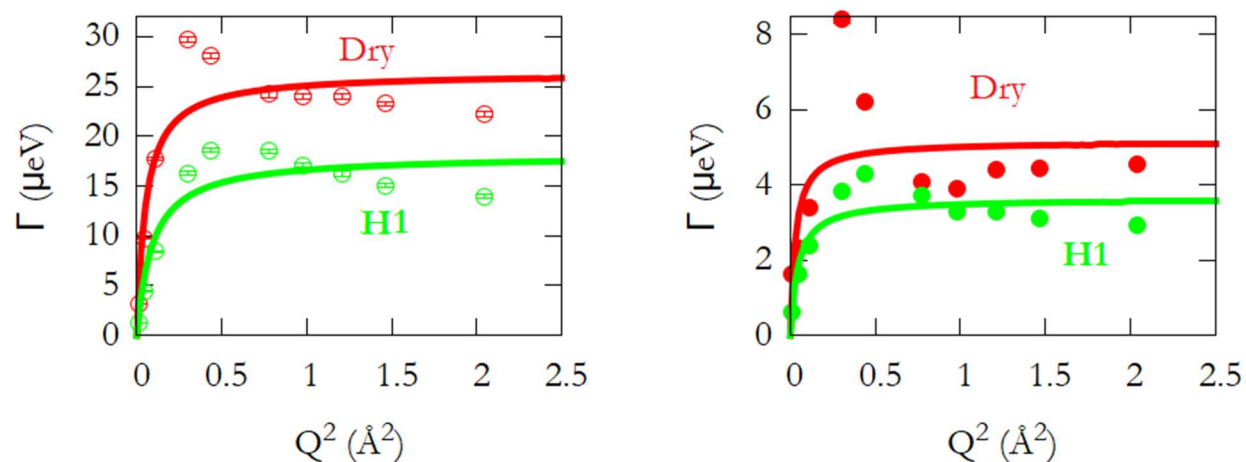
435

436   **Figure 9**. Energies ($\Gamma^s_i(Q)$ (i=1, 2)) involved in the motion represented by the simulation-derived

437   TISF in the time range 3-60 ps (left) and 100-200 ps (right). The solid lines are fits to the data

438   obtained using the jump diffusion model. The fast component of the motion is represented by

439    $\Gamma^s_1(Q)$ in the left panel, while the slow component is represented by $\Gamma^s_2(Q)$ in the right panel. In

440   the right panel, the error bars are smaller than the symbols used to show the data.

441

442   **Table 3**. Parameters of jump diffusion obtained from the fitting shown in Figure 9.

System-Component	D ($\times 10^{-10}$m^2/s)	τ (ps)
Dry-Fast	77.0±30.4	25.0±1.7
Dry-Slow	26.5±24.5	127.8±17.3
H1-Fast	30.5±11.4	36.3±2.8
H1-Narrow	12.4±5.2	181±12.6

443

444   Figure 10 shows a comparison of the RCF calculated from simulations of different composition.

445   The time range accessible to BASIS is highlighted in color. The effect of water content on the

446   rotational motion of propane is qualitatively the same as that on the translational motion, i.e., water

447   suppresses rotational motion. Further, the RCF for all compositions, except the two highest water

448   contents, decay completely before the lower limit of the time scales accessible with the instrument.

449   This shows that if a QENS experiment were carried out on these compositions using BASIS, the

450   rotational motion of propane will not contribute to the quasielastic spectra in all, but the two

451   highest water content compositions.

452
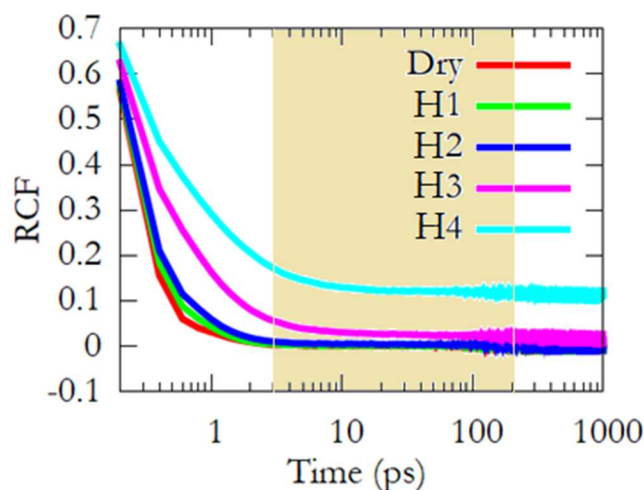
453

454   **Figure 10**. Rotational correlation function (RCF) of propane in different simulations. The time

455   range accessible to the instrument BASIS is highlighted in colour.

5. Discussion

456

457   We report diffusion coefficients of propane confined in dry and hydrated pores of MCM-41-S

458   using experimental and computational approaches. Although quantitative differences exist

459   between the results from the two techniques, the order of magnitudes and trends in the self-

460   diffusion coefficient observed are very similar. For bulk propane at saturation vapor pressure,

461   Schmid et al.[46] reported self-diffusion coefficients of 54.4×10^{-10} and 73.9×10^{-10} m^2/s at 228 K and

462   249 K, respectively. The values obtained here for propane confined in a dry MCM-41-S pore are

463   comparable to these values. We note that in our experiments, confined propane remains in the

464   vapor phase even at the lower temperatures probed. The effect of confinement due to the MCM-

465   41-S pores seems to correspond to an increase in pressure, which would imply an increase in

466   density for the confined fluid, consistent with many simulation results[47].

467   The values of residence times obtained experimentally and from the simulation derived-TISF

468   (Figure 4 and Table 3) are rather high, especially for the slower component of motion and in the

469   presence of water. For example, compared to ethane in CPG[10] and propane in silica aerogel[13], the

470   residence times obtained for propane in MCM-41-S are a factor of 3-4 higher for the fast

471   component and, in some cases, even 2 orders of magnitude higher for the slow component. We

472   note that the diffusive properties of propane in silica aerogel[13] were measured using the same

473   instrument used here, implementing the same settings of elastic resolution and energy window.

474   The slow component measured in the present study thus exhibits remarkably high residence times,

475   implying very strong intermolecular interactions, especially when water is present. The slow

476   component might represent a motion where a propane molecule shuttles within a small region for

477   a long time (i.e., the residence time), and then occasionally overcomes a high potential barrier to

478   jump to a distant site. The shuttling motion in between jumps is too fast to be captured by the

479   BASIS instrument. It is this fast shuttling motion that is represented by the very short time fast

480   decay of the TISF smaller than $\sim$ 3 ps shown in Figure 8.

481   Although the residence times of the two populations of propane molecules are very different from

482   each other, the differences in the corresponding diffusion coefficients are relatively small.

483   However, the existence of two different motions is indicated by an analysis of the scattering law

484   or the intermediate scattering functions, while the simulated mean square displacement profiles

485   yield only an averaged result. Because the Q variations of the energies involved in propane motions

486   ($\Gamma_i(Q)$ from the experiments and $\Gamma^s_i(Q)$ from the simulations) indicate diffusion occurring via

487   jumps, the results were fitted with the Singwi-Sjölander jump diffusion model. In this model, the

488   variation of $\Gamma(Q)$ with Q^2 exhibits an initial fast growth close to a straight line, followed by a

489   plateau. The slope of the initial growth period determines the diffusion coefficient, while the value

490   at the plateau determines the residence times. As the number of data points in the D-determining

491   low Q region is small in both simulations and experiments, the estimated D is more prone to errors

492   than τ. This problem is further aggravated in the slow component, as the $\Gamma(Q)$ values obtained

493   representative of this component are themselves prone to larger errors. This is because of the

494   difficulty involved in measuring a smaller quantity, especially in the presence of a larger quantity.

495   This experimental uncertainty might explain the counter-intuitive enhancement of motion at 230

496   K compared to 250 K for the slow component of the hydrated sample, while the temperature

497   variation by the MSD-derived D follows expectations.

498   The effect of water on the dynamics of confined propane is similar to that reported at 300 K in an

499   earlier publication[35]. However, the effect reported here is very different to that reported for CO_2

500   on the dynamics of confined ethane[10], propane[13], butane[30] and octane[29]. CO_2 was found to enhance

501   the mobility of the confined hydrocarbons in all these studies. This enhancement ('molecular

502   lubrication') was explained by preferential adsorption of CO_2 to the pore walls, which results in

503   the CO_2 molecules pushing the hydrocarbon molecules away from the pore surface, and thereby

504   reducing their energy barrier for diffusion[30]. Also, in the present study water was found to displace

505   propane molecules away from the pore wall. However unlike in the case of CO_2, the displacement

506   of propane from the pore surface by water resulted in a lowering of the propane diffusion

507   coefficient, possibly because of the formation of barriers to propane diffusion due to the formation

508   of hydrogen-bonded networks of water molecules that span the entire pore width, as discussed

509   below.

510   The size and geometry of the pores seem to be important factors, as well as the strong water-water

511   preferential interactions (i.e., hydrogen bonds) [48]. The pore size of MCM-41-S sample used here

512   is smaller than the pores used in the experimental studies reported in refs. 10 and 13 by factors of

513   ~ 5 and 12, respectively. Although the pore size used in refs. 29 and 30 of ~ 2nm was comparable

514   to the present case (~1.5 nm), the pore geometry was significantly different. In the MCM-41-S

515   pore, the sorbents are constrained to move within a cylinder of diameter 1.5 nm, resulting in a free

516   motion only along one dimension. In refs. 29 and 30, a slit pore was used, hence the fluid motion
517   was constrained in one direction and free within a 2-dimensional plane. This means that both the
518   cylindrical pore geometry as well as its smaller diameter result in a more crowded environment
519   for the adsorbate. These geometrical effects favour the formation of water bridges within the
520   narrow pores, especially at high water loadings. Thus, although water displaces propane from the
521   pore surface, the overall effect of increasing water content is to increase crowding and strongly
522   suppressing the mobility of confined propane.

523   Our results show that the rotational motion of confined propane molecules also exhibits
524   suppression by hydration, which is possibly due to the restricted pore volume available to propane
525   once water enters the MCM-41-S pores. The simulation data show that the rotational motions of
526   propane in all but the two highest water contents are too fast to contribute to the experimental
527   quasielastic spectra. This is consistent with the experiments, where the small values of EISF
528   obtained from fitting the QENS spectra of all samples indicate absence of any localized motion,
529   including the rotational motion. Further, in the two highest water content simulations, the RCF of
530   propane do not decay to zero even after 1 ns. This residual correlation in the orientation of the
531   propane molecules at times separated by long intervals indicates that propane molecules are unable
532   to trace the entire orientational space available to them. This is due to water molecules, which
533   block the rotation of propane at high water contents. MD study of this system at higher temperature
534   showed that water blocks propane mobility by forming molecular bridges[35]. This reduced mobility
535   in translational motion gives rise to inhomogeneities in the density distribution of propane along
536   both axial as well as radial directions at high water contents (Figure 5). A similar reduction in
537   orientational motion gives rise to orientational ordering of propane molecules at high water
538   contents (see Fig. S2 in the Supplementary Information). It is likely that the elongated geometry
539   of one propane molecule enhances the reduction of its rotational dynamics when water content
540   increases.

541   QENS experiments have been conducted at conditions such that the confined propane always
542   remains in the vapour state. Although the experimental temperature is lower than what is expected
543   in the subsurface, the thermodynamic state of propane is similar (i.e., propane remains in the vapor
544   phase). Therefore, the results presented are of relevance to practical situations encountered in the

545 subsurface, where hydrocarbons can be found in water-bearing-porous networks composed of
546 silica-rich substrates.

547

548

6. Conclusions

550 We have used a combination of quasielastic neutron scattering (QENS) experiments and molecular
551 dynamics (MD) simulations to study the effect of water on the dynamics of propane confined in
552 MCM-41-S cylindrical pores of diameter 1.5 nm. Both experiments and simulations show that
553 presence of water suppresses the mobility of propane. MD simulations show that this effect is
554 dependent on the amount of water in the pore. At the highest water content, both structure and
555 dynamics, translational as well as rotational, of confined propane are severely constrained. Water
556 is found to displace propane molecules from the pore surface. A similar mechanism involving CO_2
557 has been found to enhance the diffusivity of several hydrocarbons, including propane. In the
558 present case though, the effects of displacement of propane from the pore surfaces are countered
559 by an increased molecular crowding, which is due to a combination of small pore diameter,
560 cylindrical pore geometry, and strong water-water hydrogen bonds. The resultant effect is an
561 overall suppression of propane mobility. The mechanism of propane diffusion does not however
562 seem to be affected by the presence of water, at least at moderate water loadings. Our simulations
563 suggest that above a water-loading threshold propane becomes trapped within the hydrated pores,
564 at least for the time scales accessible to our MD simulations. Although the measurements reported
565 here were made at low temperatures of 230 and 250 K, propane was at low pressure and in the
566 vapor phase. Thus, the present study could have implications for the subsurface environment where
567 hydrocarbons in vapor phase are found trapped in water saturated porous networks even at
568 geologic temperatures.

569

7. Acknowledgements

585

586   8. Conflict of Interest

587   The authors declare that there is no conflict of interest.

588

589   9. References

590 [1] Cole, D. R., Mamontov, E. and Rother, G. in Liang, L., Rinaldi, R. and Schoeber, H., (Eds.)

591 Neutron Applications in Earth, Energy, and Environmental Sciences, **2009**, 547-570.

592 [2] Wang, H., Wang, L., He, S., & Xiao, F. S. "Enhancement of Catalytic Properties by

593 Adjusting Molecular Diffusion in Nanoporous Catalysts." In C. Song (Ed.) Advances in

594 Catalysis, Vol. 62, 1-46, Academic Press, **2018**.

595 [3] Demontis, P., Suffritti, G. B. Structure and dynamics of zeolites investigated by molecular

596 dynamics. *Chem. Rev.*, **1997**, *97(8)*, 2845-2878.

597 [4] Hahn, K., Karger, J. and Kukla, V. Single-File Diffusion Observation, *Phys. Rev. Lett*., **1996**,

598 *76*, 2762-2765.

599 [5] Bhide, S. Y. and Yashonath, S. Dependence of the Self-Diffusion Coefficient on the Sorbate

600 Concentration: A Two-Dimensional Lattice Gas Model With and Without Confinement, *J.*

601 *Chem. Phys.,* **1999**, *111*, 1658-1667.

602 [6] Bhide, S. Y. and Yashonath, S. Types of Dependence of Self-Diffusivity on Sorbate

603 Concentration in Parameter Space: A Two-Dimensional Lattice Gas Study, J. Phys. Chem. B,

604 **2000**, *104*, 2607-2612.

605 [7] Gautam, S., Ok, S., and Cole, D. R. Structure and Dynamics of Confined C-O-H Fluids

606 Relevant to the Subsurface: Application of Magnetic Resonance, Neutron Scattering and

607 Molecular Dynamics Simulations, Front. In Earth Sc. **2017** 5:43. doi: 10.3389/feart.2017.00043

608 [8] Cole, D. R., Grszkiewicz, M. S., Simonson, J. M., Chialvo, A. A., Melnichenko, Y. B.,

609 Wignall, G. D., Lynn, G. W., Lin, J. S., Habenschuss, A., Gu, B., et al., "Influence of Nanoscale

610 Porosity on Fluid Behavior" In: Water-Rock Interaction, 737-740, (Wanty, R. B. and Seal II, R.

611 R. Eds.) Taylor & Francis, London **2004.**

612 [9] Chathoth, S. M., Mamontov, E., Melnichenko, Y. B. and Zamponi, M. Diffusion and

613 Adsorption of Methane Confined in Nano-Porous Carbon Aerogel: A Combined Quasi-Elastic

614 and Small-Angle Neutron Scattering Study, *Micro. Meso. Mater.,* **2010**, *132*, 148-153.

615 [10] Patankar, S., Gautam, S., Rother, G., Podlesnyak, A., Ehlers, G., Liu, T., Cole, D. R., and

616 Tomasko, D. L. Role of Confinement on Adsorption and Dynamics of Ethane and an Ethane-

617 CO_2 Mixture in Mesoporous CPG Silica, *J. Phys. Chem. C* **2016**, *120*, 4843-4853.

618 [11] Gautam, S., Liu, T., Patankar, S., Tomasko, D., & Cole, D. Location dependent orientational

619 structure and dynamics of ethane in ZSM5. *Chem. Phys. Lett.*, **2016**, *648*, 130-136.

620 [12] Gautam, S., and Cole, D., Molecular Dynamics Simulation Study of Meso-Confined

621 Propane in TiO_2, *Chem. Phys.* **2015**, *458*, 68 – 76.

622 [13] Gautam, S., Liu, T., Rother, G., Jalarvo, N., Mamontov, E., Welch, S., Sheets, J., Droege,

623 M., and Cole, D. R. Dynamics of Propane in Nanoporous Silica Aerogel: A Quasielastic Neutron

624 Scattering Study, *J. Phys. Chem. C*, **2015**, *119*, 18188-18195.

625   [14] Stepanov, A. G., Shegai, T. O., Luzgin, M. V., and Jobic, H. Comparison of the dynamics of

626   n-hexane in ZSM-5 and 5A zeolite structures. *The European Physical Journal E*, **2003**, *12*, 57-

627   61.

628   [15] Gautam, S., Mitra, S., Mukhopadhyay, R. and Chaplot, S. L. Diffusion of Acetylene inside

629   Na-Y Zeolite: Molecular Dynamics Simulation Studies, *Phys. Rev. E*, **2006**, *74*, 041202.

630   [16] Sharma, V. K., Gautam, S., Mitra, S., Rao, M. N., Tripathi, A. K., Chaplot, S. L. and

631   Mukhopadhyay, R., Dynamics of Adsorbed Hydrocarbon in Nanoporous Zeolite Framework, *J.*

632   *Phys. Chem. B*, **2009**, *113*, 8066-8072.

633   [17] Gautam, S., Sharma, V. K., Mitra, S., Chaplot, S. L., & Mukhopadhyay, R. Rotational

634   dynamics of propylene in ZSM-5 zeolitic frameworks. *Chem. Phys. Lett.*, **2011,** *501*, 345-350.

635   [18] Gautam, S., Mitra, S., Sayeed, A., Yashonath, S., Chaplot, S. L., & Mukhopadhyay, R.

636   Diffusion of 1, 3-butadiene adsorbed in Na–Y zeolite: Neutron scattering study. *Chem. Phys.*

637   *Lett.*, **2007,** *442*, 311-315.

638   [19] Gautam, S., Mitra, S., Chaplot, S. L. and Mukhopadhyay, R. Dynamics of 1,3-Butadiene

639   Adsorbed in Na-Y Zeolite: MD Simulation Study, *Phys. Rev. E*, **2008**, *77*, 061201.

640   [20] Thalladi, V. R., & Boese, R. Why is the melting point of propane the lowest among n-

641   alkanes?. *New J. Chem.*, **2000**, *24*, 579-581.

642   [21] Mukhopadhyay, R., Sayeed, A., Mitra, S., Kumar, A. V. A., Rao, M. N., Yashonath, S. and

643   Chaplot, S. L. Rotational Dynamics of Propane in Na-Y Zeolite: A Molecular Dynamics and

644   Quasielastic Neutron Scattering Study, *Phys. Rev. E,* **2002**, *66*, 061201

645   [22] Le, T., Striolo, A., and Cole, D. R. Propane Simulated in Silica Pores: Adsorption

646   Isotherms, Molecular Structure, and Mobility, *Chem. Eng. Sci.* **2015**, *121*, 292-299.

647   [23] Gautam, S., Le, T., Striolo, A., and Cole, D. Molecular dynamics simulations of propane in

648   slit shaped silica nano-pores: direct comparison with quasielastic neutron scattering experiments.

649   *Phys. Chem. Chem. Phys.*, **2017,** *19*, 32320-32332.

650 [24] Dhiman, I., Shrestha, U. R., Bhowmik, D., Cole, D. R., and Gautam, S. (2019). Influence of
651 molecular shape on self-diffusion under severe confinement: A molecular dynamics study. *J.*
652 *Chem. Phys.*, **2019**, *516*, 92-102.

653 [25] Dhiman, I., Bhowmik, D., Shrestha, U. R., Cole, D. R., & Gautam, S. Effect of molecular
654 shape on rotation under severe confinement. *Chem. Eng. Sc.*, **2018**, *180*, 33-41.

655 [26] Gautam, S.; Kolesnikov, A. I.; Rother, G.; Dai, S.; Qiao, Z. A.; Cole, D. Effects of
656 Confinement and Pressure on the Vibrational Behavior of Nano-Confined Propane. *J. Phys.*
657 *Chem. A* **2018**, *122*, 6736–6745.

658 [27] Chathoth, S. M.; He, L.; Mamontov, E.; Melnichenko, Y. B. Effect of Carbon Dioxide and
659 Nitrogen on the Diffusivity of Methane Confined in Nano-Porous Carbon Aerogel. *Microporous*
660 *Mesoporous Mater.* **2012***, 148*, 101-106.

661 [28] Salles, F.; Jobic, H.; Devic, T.; Guillerm, V.; Serre, C.; Koza, M. M.; Ferey, G.; Maurin, G.
662 Diffusion of Binary CO_2/CH_4 Mixtures in the MIL-47(V) and MIL-53(Cr) Metal – Organic
663 Framework Type Solids: A Combination of Neutron Scattering Measurements and Molecular
664 Dynamics Simulations. *J. Phys. Chem. C* **2013***, 117*, 11275-11284.

665 [29] Le, T.; Ogbe, S.; Striolo, A.; Cole, D. R. N-octane diffusivity enhancement via carbon
666 dioxide in silica slit-shaped nanopores – a molecular dynamics simulation. *Mol. Simul.* **2016***, 42*,
667 745−752.

668 [30] Le, T., Striolo, A., Cole, D. R. CO_2–C_4H_{10} mixtures simulated in silica slit pores: relation
669 between structure and dynamics. *J. Phys. Chem. C,* **2015**, *119*(27), 15274-15284.

670 [31] Chakraborty, S., Kumar, H., Dasgupta, C. Maiti, P. K. Confined water: Structure,
671 dynamics, and thermodynamics. *Acc. Chem. Res.*, **2017**, *50*, 2139-2146.

672 [32] Cerveny, S., Mallamace, F., Swenson, J., Vogel, M., Xu, L. Confined water as model of
673 supercooled water. *Chem. Rev.*, **2016**, *116*, 7608-7625.

674 [33] Phan, A., Cole, D. R., Weiß, R. G., Dzubiella, J., Striolo A. Confined water determines
675 transport properties of guest molecules in narrow pores. *ACS Nano*. **2016,** *10*, 7646 – 7656.

676   [34] Bui T., Phan A., Cole D. R., Striolo A. Transport Mechanism of Guest Methane in Water-

677   Filled Nano-Pores. *J. Phys. Chem. C* **2017**, *121*, 15675 – 15686.

678   [35] Le, T. T. B., Striolo, A., Gautam, S. S., Cole, D. R. Propane–water mixtures confined within

679   cylindrical silica nanopores: structural and dynamical properties probed by molecular dynamics.

680   *Langmuir*, **2017**, *33*, 11310-11320.

681   [36] Mamontov, E.; Herwig, K. W. A Time-of-Flight Backscattering Spectrometer at the

682   Spallation Neutron Source, BASIS. *Rev. Sci. Instrum.* **2011***, 82*, 085109.

683   [37] Azuah, R. T.; Kneller, L. R.; Qiu, Y.; Tregenna-Piggott, P. L. W.; Brown, C.M.; Copley, J.

684   R. D. Dimeo,R.M. DAVE: A Comprehensive Software Suite for the Reduction, Visualization,

685   and Analysis of Low Energy Neutron Spectroscopic Data. *J. Res. Natl. Inst. Stand. Technol.*

686   **2009**, *114*, 341−358.

687   [38] Demiralp, E.; Cagin, T.; Goddard, W. A. Morse stretch potential charge equilibrium force

688   field for ceramics: Application to the quartzstishovite phase transition and to silica glass. *Phys.*

689   *Rev. Lett.* **1999**, *82 (8)*, 1708-1711.

690   [39] Cygan, R. T.; Liang, J. J.; Kalinichev, A. G. Molecular models of hydroxide, oxyhydroxide,

691   and clay phases and the development of a general force field. *J. Phys. Chem. B* **2004**, *108 (4)*,

692   1255-1266.

693   [40] Abascal, J. L. F., Sanz, E., García Fernández, R., & Vega, C. A potential model for the

694   study of ices and amorphous water: TIP4P/Ice. *J. Chem. Phys.* **2005,***122(23)*, 234511.

695   [41] Martin, M. G.; Siepmann, J. I. Transferable potentials for phase equilibria. 1. United-atom

696   description of n-alkanes. *J. Phys. Chem. B* **1998**, *102 (14), 2569-2577.

697   [42] Essmann, U.; Perera, L.; Berkowitz, M. L.; Darden, T.; Lee, H.; Pedersen, L. G. A Smooth

698   Particle Mesh Ewald Method. *J. Chem. Phys.* **1995**, *103 (19)*, 8577-8593.

699   [43] Allen, M. P.; Tildesley, D. J. *Computer Simulation of Liquids* Oxford University Press:

700   Oxford, U.K., **2004**.

701   [44] M. Bee, *Quasielastic Neutron Scattering,* Adam Hilger, Bristol, **1988**.

702 [45] Singwi, K. S.; Sjölander, A. Diffusive Motions in Water and Cold Neutron Scattering. *Phys.*

703 *Rev.* **1960**, *119*, 863-871

704 [46] Greiner-Schmid, A.; Wappmann, S.; Has, M.; Lüdemann, H. D.Self-Diffusion in the

705 Compressed Fluid Lower Alkanes: Methane,Ethane, and Propane. *J. Chem. Phys.* **1991**, *94*,

706 5643-5649.

707 [47] Cole, D. R. and Striolo, A. (2019) Chapter 12. The Influence of nanoporosity on the

708 behavior of carbon-bearing fluids. In: *Deep Carbon: Past and Present*. (editors – B. Orcutt, I.

709 Daniel, R. Dasgupta), Cambridge University Press, 358-387.

710 [48] Ho, T. A., Striolo, A. Water and methane in shale rocks: Flow pattern effects on fluid

711 transport and pore structure. *AIChE Journal*, **2015,** *61*(9), 2993-2999.

712
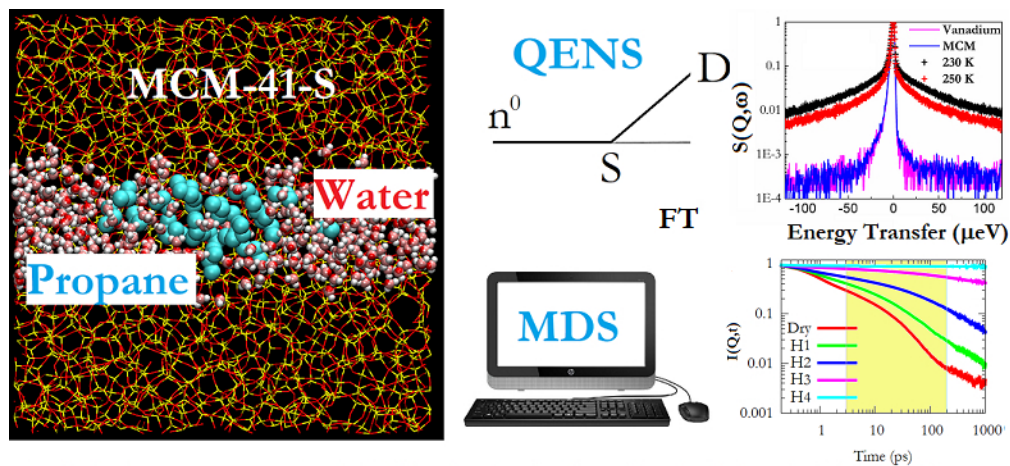
Quasi-elastic neutron scattering (QENS) and molecular dynamics simulations (MDS) reveal the effects of water on the structure and dynamics of propane confined in 1.5 nm wide cylindrical pores of MCM-41-S